Journal of Electronic Materials, Vol. 4, No. 5, 1975

EXCITED STATE POLARIZATION, BULK PHOTOVOLTAIC EFFECT AND THE PHOTOREFRACTIVE EFFECT IN ELECTRICALLY POLARIZED MEDIA

A. M. Glass, D. von der Linde, D. H. Auston and T. J. Negran

Bell Laboratories
Murray Hill, New Jersey 07974

(Received March 25, 1975)

Optical absorption in pyroelectric crystals is accompanied by electrical effects (in addition to the well-known pyroelectric effect) which are not present in other materials. Optical excitation between localized states gives rise to an instantaneous macroscopic polarization change due to the change of dipole moment at the absorbing center. Excitation of free carriers from localized states will in general result in a bulk photovoltaic effect due to asymmetric charge transfer. Thus spatially non-uniform illumination gives rise to internal fields, resulting in refractive index variations. Studies of these effects for fast detection, optical logic, memories, and microwave generation will be described.

Key words: excited state dipoles, photovoltaic effects, optically induced index changes.

Introduction

Over the past several years there have been many reports of unusual photoeffects in ferroelectrics, pyroelectrics and other electrically polarized materials. For instance Chynoweth (1) observed steady state photocurrents

in $BaTiO_3$ when crystals were illuminated with radiation of wavelength shorter than the bandgap, which were related to, but distinct from, the pyroelectric effect in these crystals. Larger than bandgap photovoltages were observed in several asymmetric polycrystalline materials: Lempiki (2) noted that in striated ZnS crystals the photovoltage was always in the direction of the pyroelectric axis and in $BaTiO_3$ ceramics Brody (3) found that the photovoltage was related to the magnitude of the remanent polarization. To account for his observations of optically induced refractive index changes in single crystal $LiNbO_3$, Chen (4) found it necessary to postulate the presence of internal fields up to 10^5 V/cm within the bulk of the crystal.

In this paper we will discuss how electronic excitation of defects in pyroelectric crystals can give rise to electrical effects which are not present in other materials and attempt to account for the anomalous behavior just described.

II. Excited State Polarization

The spontaneous polarization P_s of a pyroelectric may be written

$$P_s = \frac{\mu}{V_u} = N\Sigma e_i \bar{x}_i \qquad .. 1$$

where V_u is the unit cell volume, μ is the dipole moment per unit volume and $\bar{x}_i$ is the displacement of the ith ion of the unit cell from a center of symmetry. Any change of polarization from the equilibrium value due to a change of μ or V_u results in a field across the crystal which can be measured externally under open circuit conditions ($\Delta D = 0$), or if the surfaces are short circuited ($\Delta E = 0$) the current density

$$J = dP/dT \qquad .. 2$$

in the external circuit can be measured. Thermal excitation of a crystal results in pyroelectric polarization due to thermal expansion (change of V_u) and atomic displacement (change of μ). What is not

so well known, however, is that electronic excitation also gives rise to a polarization change due to the change of dipole moment $\Delta\mu_e$ associated with the absorbing center upon excitation.

$$\Delta P = n\Delta\mu_e \qquad .. 3$$

where n is the density of excited electrons. The origin of this change of electronic dipole moment with transitions between localized states in an asymmetric potential is clarified in Figure 1. For simplicity a triangular shaped potential is chosen since the solution of Schrodingers Equation for this potential is well known (5). The eigenstates and eigenfunctions are shown in the figure. The center of charge $\langle\psi_i|x|\psi_i\rangle/\langle\psi_i|\psi_i\rangle$ in the ground and excited states is marked with arrows showing clearly the displacement upon excitation. For instance for a local field of 10^8 V/cm, $\Delta\mu \sim 9$ Debye. While such a displacement occurs in any asymmetric potential, only in pyroelectric hosts does the displacement have the same sense at all

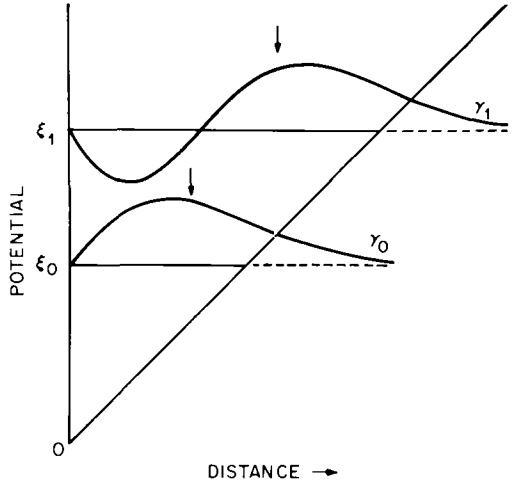

Fig. 1. The two lowest energy eigenstates and eigenfunctions of a triangular potential well. Arrows indicate the center of charge in each state.

equivalent centers resulting in a macroscopic polarization change.

At a defect site in a pyroelectric crystal the situation is more complicated than an isolated set of one-electron states. For instance the magnitude of the dipole moment depends not only on the local field and the electronic configurations but also on vibrational-electronic interaction, and dipole induced polarization of the surrounding crystal. Non-radiative electronic relaxation results in heating of the lattice and hence an additional pyroelectric contribution to the polarization. For a two level adiabatic system, the total polarization change, neglecting piezoelectric effects is given by

$$\frac{\partial P}{\partial t} + \frac{P}{\tau} \approx \Delta\mu \frac{dn}{dt} + \frac{p}{\tau} \Delta T \qquad .. 4$$

where p is the pyroelectric coefficient and T the temperature. For uniform excitation of the crystal with light intensity I(t) and photon energy $h\nu$ this equation can be written

$$\frac{dP}{dt} + \frac{P}{\tau} = \frac{\alpha\Delta\mu}{h\nu} I(t) + \alpha(1-e) \frac{p}{C\tau} \int I(t)dt \qquad .. 5$$

where e is the radiative quantum efficiency, α the absorption coefficient and C the thermal capacity of the crystal. Measurement of the polarization change following excitation of a particular defect should therefore afford a direct measurement of $\Delta\mu$ provided the lifetime τ of the state is long enough. Excitation with mode locked lasers implies $\tau > 10^{-11}$ seconds. In effect this is the reverse of a Stark effect measurement where the local asymmetry is provided by the external field.

Experimental measurement (6) of the polarization change following excitation of the $^4T_2$ state of the Cr^{3+} ion in $LiNbO_3$ with optical pulses of duration much less than the excited state lifetime, yielded a magnitude of $\Delta\mu \sim 3$ Debye.

A similar experiment (7) was performed with Nd^{3+} ions in $LiNbO_3$ (excitation of the $^4G_{5/2}$ state). In this case

no excited state dipole moment was observed - just the pyroelectric polarization due to the fact that the f-states of rare earth ions are relatively insensitive to local fields.

III. Photovoltaic Effect in Homogeneous Pyroelectrics

The polarization change resulting from localized electronic transitions produces a transient current when the light is turned on or off but no steady state current with constant illumination. The electric field $E = -\Delta P/\varepsilon\varepsilon_o$ measured externally along the polar axis relaxes with the dielectric relaxation time of the material or with the RC relaxation time of the external circuit, whichever is the shorter. However, if the incident radiation has sufficient energy to photoionize the defect a steady state e.m.f. may be created due to the directional properties of the charge transfer process. Directional intervalence transfer from a substitutional cation in a pyroelectric host will occur if the overlap of defect orbitals with the host cations in the ± polar directions differ due to the local asymmetry. Following excitation the ionized impurity will in general be displaced along the polar axis due to Frank-Condon relaxation (coupling with asymmetric modes) giving additional displacement current. Consider the simple asymmetric potential shown in Fig. 2. Excitation between

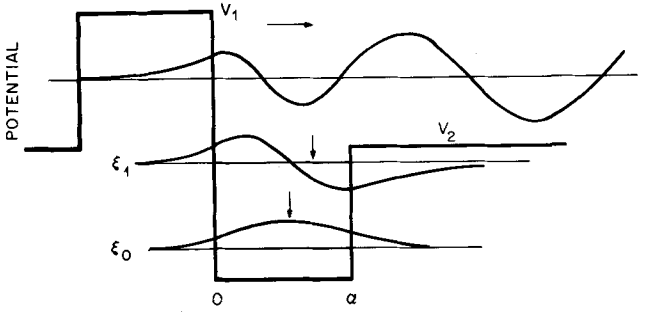

Fig. 2. Solution of Schrödingers Equation for an asymmetric rectangular potential well, showing two bound states and one free state.

bound states of energy $E < V_2$ gives electronic displacement as discussed before (center of charge marked with arrows), but on excitation to states of energy $V_1 > E > V_2$ the electron is free to move only in one direction as shown. Electrons moving in the opposite direction are at least partially reflected by the potential barrier so that even if tunnelling through the barrier is possible, the probability of electron transfer in the positive polar direction p_+ differs from that in the opposite direction p_-. If the potential is a sufficiently small perturbation of the host crystal, and slowly varying so that the effective mass approximation can be used then the free electron states may be described in terms of the conduction electron states of the host. Directional charge transfer then means that the excited electron couples differently to states of positive and negative k vectors.

Since the asymmetry has the same sense at all equivalent defects there is a net electronic current upon excitation

$$J_{e_1} = \frac{e\alpha I}{h\nu} (p_+ l_+ - p_- l_-) \qquad .. 6$$

where $l_\pm$ are the mean free paths of the electrons in the $\pm$ polar directions. In addition the displacement of the ionized impurity and surrounding ions along the polar axis following excitation gives a current

$$J_{e_2} = \frac{\alpha I}{h\nu} (Z_i \Delta l_i) \qquad .. 7$$

where Δl_i is the displacement of the ith ion of charge Z_i, and the product $Z_i \Delta l_i$ is summed over all ions.

After the electron is scattered its motion becomes isotropic and does not contribute to the photocurrent until recombination. If the probabilities of recombination at the impurity from the $\pm$ polar directions are p'_+ and p'_- then the recombination current J_r is given by similar equations to Eqn. 6,7 but with $l_\pm p_\pm$ replaced by $l'_\pm p'_\pm$ and Z_i replaced by Z'_i. Of course Δl_i is the same after both excitation and recombination since the impurity moves between two locations, but the charges Z_i are not the

same since the impurity carries an additional trapped charge after recombination.

The steady state photocurrent can be written

$$J = J_e - J_r = \kappa\alpha I$$

where

$$\kappa = \frac{e}{h\nu}\left(l_+p_+ - l_-p_- + l'_+p'_+ - l'_-p'_-\right) + \frac{Z_l - Z'_i}{h\nu}\Delta l_i \qquad .. 8$$

is a constant depending only on the nature of the absorbing center, the local environment and the photon energy.

We see from Eq. 8 that even if the probabilities of electron transfer in the positive and negative polar directions at the impurity site are the same so that the term in parentheses in Eq. 8 is zero (i.e. $V_1 = V_2$ in Fig. 2) that there is a net current due to coupling of the charged defects to asymmetric modes.

Under open circuit conditions the photocurrent charges the crystal capacitance generating a macroscopic electric field E given by

$$J = \kappa\alpha I + \sigma E \qquad .. 9$$

where σ is the electrical conductivity of the crystal during illumination, so that in the steady state the saturation field

$$E_{sat} = \kappa\alpha I/\sigma \qquad .. 10$$

In principle κ is itself a function of E since the microscopic potential at the defect changes with E. The important feature of this photovoltaic effect which distinguishes it from conventional photovoltaic effects is firstly that it is a bulk property of homogeneous pyroelectrics (with homogeneous defect distribution). The photocurrent is driven by microscopic local fields and not a macroscopic field due to carrier concentration gradients

or gradients of crystal composition. Secondly the open circuit saturation voltage is just the product of the saturation field and the crystal length along the polar axis, and is not limited by an electronic band gap.

This photovoltaic effect is particularly evident in $LiNbO_3$ doped with Fe^{2+} impurities (8). These defects introduce absorption where the host crystal is transparent as shown in Fig. 3. The broad band at 9000 cm^{-1} is due to localized transitions between d-states of the impurity and the band near 20,000 cm^{-1} can be attributed to intervalence transfer from Fe^{2+} ions to next nearest neighbor Nb^{5+} ions (9). The intense absorption near 25,000 cm^{-1} is due to charge transfer from the oxygen ligands to Fe^{2+} and Fe^{3+} ions.

A typical photocurrent spectrum of these crystals is also shown on Fig. 3. The constant κ was obtained measuring the short circuit current along the polar axis of a uniformly illuminated crystal with zero applied field. The current was measured in the steady state

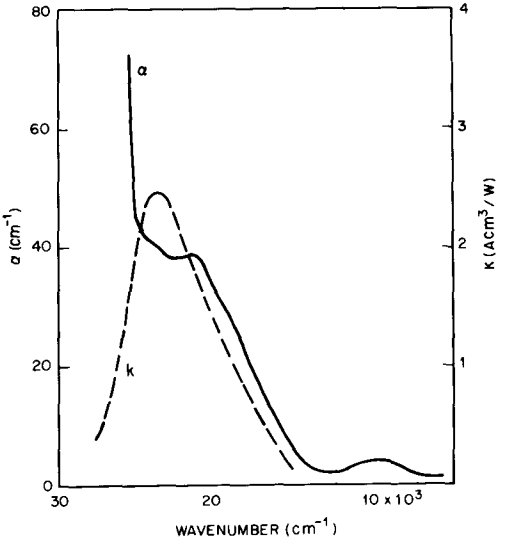

Fig. 3. Absorption spectrum and photocurrent spectrum of a $LiNbO_3:Fe^{2+}$ crystal at 300°K.

after the pyroelectric transient had decayed with the thermal relaxation time of the crystal. The value of κ calculated from the steady state component was independent of the crystal geometry, and whether the polar axis was parallel or perpendicular to the incident radiation.

No photocurrent was measured in the 9000 cm^{-1} band as expected for localized transitions. The value of κ increased at shorter wavelengths, reaching a maximum for electron transfer to the conduction band (based on Nb orbitals) and decreasing at still shorter wavelengths where charge transfer from the ligands probably becomes dominant. κ was found to be essentially independent of the Fe^{2+} concentration. For instance κ varied from about 1.8 to 3.0×10^{-9} Acm/W for a variation of absorption coefficient α from 0.3 cm^{-1} to 240 cm^{-1}. This range of κ may even be attributable to variations of the degree of poling of the $LiNbO_3$ crystals, and to experimental error. A value of $\kappa = 3\times10^{-9}$ Acm/W corresponds to a dipole moment of about 3.8 Debye, or net electron displacement of 0.8 Å per excitation.

Under open circuit conditions the saturation field was measured to be about 10^5 V/cm at 4727 Å corresponding to a voltage in excess of 10,000 volts across the crystals. For intensities greater than 10 mW/cm^2 the saturation field was independent of intensity as expected from Eq. 10 if $\sigma \propto I$, which is the case if photoconductivity is much greater than the dark conductivity (see below). However E_{sat} did depend on the Fe^{2+}/Fe^{3+} ratio of the crystals even though κ did not. This can be attributed to the variation of the electrical conductivity of crystals with defect concentration. A typical measurement of the conductance of a $LiNbO_3$ + 0.2% Fe crystal with $\alpha = 45$ cm^{-1} in external applied fields and different intensities of illumination at 4727 A is shown in Fig. 4. All the I-V characteristics are biased to positive current values by the photovoltaic effect when the crystal was illuminated. The transport properties can be described by

$$\kappa = 2.5\times10^{-9} \text{ Acm/W}$$

and $$\sigma = 1.3\times10^{-14} + 1.2\times10^{-12} \, I \text{ (ohm cm)}^{-1}$$

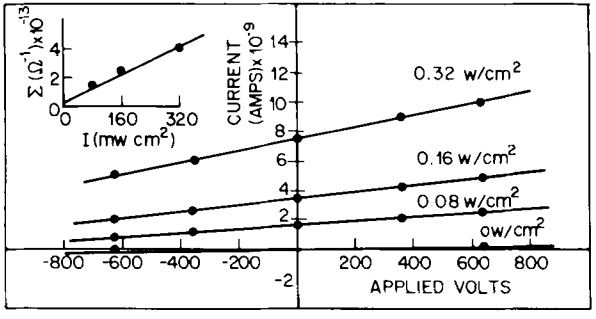

Fig. 4. Current - voltage characteristics of $LiNbO_3$:Fe at 300°K illuminated with various intensities of 0.4727 μm radiation.

where the incident intensity is in W/cm^2. In this crystal most of the Fe impurities were in the trivalent state. When a crystal of the same Fe concentration was reduced in a nitrogen atmosphere for 1 hour at 1050°C the Fe^{2+} absorption increased to 225 cm^{-1} and

$$\kappa = 2.3\times10^{-9} \text{ Acm/W}$$

and $$\sigma = 6.5\times10^{-14} + 1.5\times10^{-11} \text{ I (ohm cm)}^{-1}$$

The increase of the photoconductivity, was greater than the five fold increase of α. At high intensities where the dark conductivity is negligible we can write

$$\sigma = \frac{\alpha I}{h\nu} \tau e \mu \qquad .. 11$$

where τ is the lifetime of an excited carrier in the conduction band and μ is the mobility. The increase in photoconductivity over the ratio of α is probably due to an increase in the product μτ in the reduced crystal due to the decreased density of Fe^{3+} trapping states.

The electrical conversion efficiency per unit volume within the crystal (not a load) is given by

$$\eta = \frac{J^2}{\alpha I \sigma} = \frac{\kappa^2 \alpha I}{\sigma} = \frac{L^2 e}{\mu \tau h\nu} \qquad .. 12$$

where L = is the average charge displacement. Writing the collison rate of an electron $\tau' = m^*\mu/e$ where m^* is the effective mass we have

$$\eta = \frac{m^* L^2}{\tau \tau' h\nu} \qquad .. 13$$

This is a maximum when $\tau = \tau'$ and L is a maximum: i.e. when all photoexcited electrons move in the same direction and recombine at a neighboring defect without being scattered. The conversion efficiency when the free electron contribution to L is dominant is then

$$\eta \simeq (E - V_1)/E$$

where $E = h\nu$ (see Fig. 2).

For iron doped $LiNbO_3$ the internal efficiency is only 0.03% so this material is certainly not optimized for power conversion. It was not possible to determine whether conduction electron or ionic displacement was dominant.

IV. Photovoltaic Effects in Inhomogeneous Pyroelectrics

The high voltage photovoltaic effect described in the preceding section is a bulk property of homogeneous materials and is not dependent on optical intensity gradients or surface effects. In this respect the effect must be distinguished from other photovoltaic effects. For instance the Dember effect arises from non-uniform absorption of light and the photovoltage generated is due to the differences of electron and hole diffusion rates in the concentration gradient. Macroscopic inhomogeneities which cause band bending can give rise to photovoltages due to the drift of photoexcited carriers in the space charge region. In a similar manner

a polarization variation in a pyroelectric arising from non-uniform absorption can cause band bending and photovoltaic effects (10). However in all these cases the maximum steady state photovoltage is the value of the electronic bandgap.

This is not the case for inhomogeneous pyroelectrics such as polycrystalline films and ceramics. In these materials, under certain circumstances the smaller-than-bandgap photovoltages generated across individual grains may be additive so that the accumulated voltage across an entire specimen may greatly exceed the bandgap. The anomalously high photovoltages observed in sputtered ZnS films, (11) striated ZnS crystals, (12) various $BaTiO_3$ ceramics (3) and several other materials have been attributed to this kind of effect.

The one-dimensional layer structure of Fig. 5 shows how the photovoltage across individual grains can be additive. If both A and B components of the structure

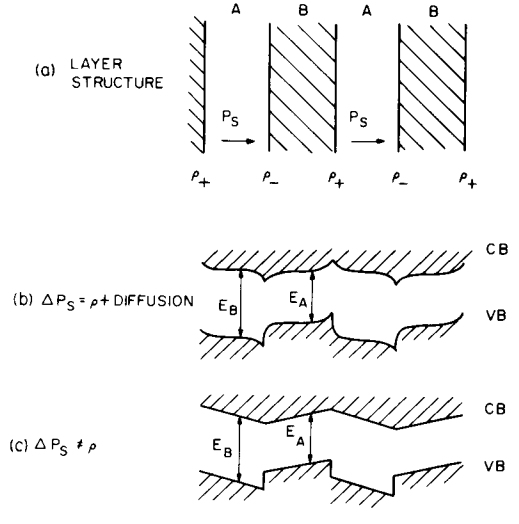

Fig. 5. a) One dimensional layer structure representing polycrystalline materials b) band structure when P_S is compensated by free charge c) band structure when P_S is not compensated.

have a center of symmetry then any voltage due to band bending at an AB junction will be exactly canceled by that at the BA junction and the voltage across the entire structure cannot exceed that across a single junction. If however either A or B or both are pyroelectric then the AB and BA junctions are no longer equivalent. For simplicity suppose that A is pyroelectric and B is centric and the polar axis of the A region has the same sense through the entire structure. This is the case of striated ZnS crystals where A has a hexagonal structure and B is cubic. At the junction between the positive ($+P_s$) end of A and B there is an accumulation of negative charge to compensate for the depolarization fields in order that the normal component of D be continuous at the interface. At the junction of the $-P_s$ end of A and B there is a deficiency of negative charge. In general the charge will diffuse both sides of the interface causing bending of the valence and conduction bands as shown in Fig. 5b, in addition to any band bending due to mismatch of the Fermi levels of A and B. Even if both materials are perfect insulators so that no free charge can accumulate at the interface (although this is not realistic under illumination) the depolarizing fields in A and B will give band bending as shown in Fig. 5c. In either case non-equilibrium carriers excited by light of wavelength shorter than the bandgap of either A or B or both, will drift under the influence of the fields such that there is a net photovoltage across an AB layer pair. The saturation photovoltages of about 0.1 V per AB pair have been calculated for ZnS for the case of uniform fields (Fig. 5c) by Neumark, (13) which is roughly consistent with the experimental estimate of Merz. (12) This model predicts that the sign of the photovoltage will change with wavelength since at longer wavelengths only the B region is absorbing and the photovoltage is in the $-P_s$ direction while at shorter wavelengths both A and B absorb and a photovoltage of the opposite sign is expected.

With such a model the external photovoltage should be directly proportional to the number of laminations of the structure. Although such a correlation was reported by Merz, (12) subsequent measurements (14) were unable to confirm such a correlation - indeed any correlation seemed weak. In view of these reports it

seems possible that both the bulk photovoltaic effect due to the presence of defects discussed in the last section as well as the additive junction effects of this section may be playing significant roles. The relative importance of the two effects will depend on several parameters including details of the polarization compensation at crystallite boundaries, the material conductivity and the nature of the defects in the material.

Anomalous photovoltages have also been observed in non-pyroelectric but piezoelectric CdTe films. (15) A similar explanation may be used to account for this observation provided that strains at the grain boundaries generate a piezoelectric polarization with specific orientation. (16)

In ferroelectric ceramics it is possible to control the gain size during preparation and the magnitude of the net polarization during poling of the material. In this case the structure is not the regular laminated structure shown in Fig. 10 but the principle remains the same: Neighboring grains have differing polarization vectors in so that div $P \neq 0$ at the boundary and hence a different absorption edge in the polar direction of the ceramic. Studies of $BaTiO_3$ ceramics (3) have shown that the photovoltage depends directly on the net polarization and the grain size of the ceramic. Similar effects are observed in PLZT (lanthanum doped lead zirconate-titanate) ceramics. (17) Figure 6 shows the wavelength dependence of the photovoltage, current and photoconductivity of a hot pressed PLZT ceramic. Because of severe scattering, meaningful absorption measurements were difficult to obtain. However at wavelengths shorter than 0.45 μm all the incident radiation was absorbed by the ceramic. Since the zero field photocurrent was proportional to the incident intensity it is still possible to describe the behavior by Eq. 9. The saturation open circuit voltage was measured to be about 200 V which is consistent with the ratio of photovoltaic current to photoconductance (Eq. 10). From these experiments therefore it is not possible to determine the relative importance of junction effects and bulk photovoltaic effects due to homogeneously distributed defects.

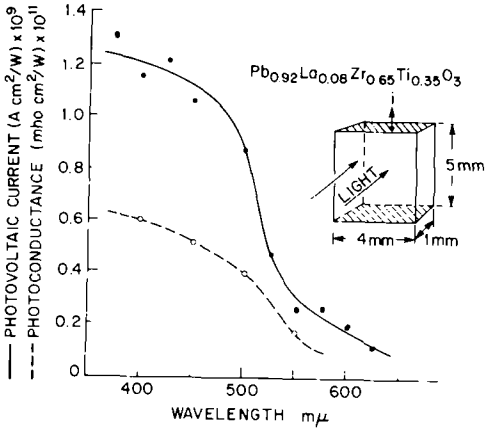

Fig. 6. Photovoltaic current response i/I and photoconductance of a PLZT ceramic at 300°K.

V. The Photorefractive Effect

In addition to the optically generated currents described in the preceding sections, non-uniform illumination may give rise to free carrier transport by diffusion in a concentration gradient:

$$J = eD_e dn/dx \qquad .. 14$$

where D_e is the diffusion coefficient. The total transport equation for monochromatic excitation is then

$$J = \kappa\alpha I + \sigma E + eD_e\frac{dn}{dx} + p\frac{dT}{dt} + \Delta\mu_i\frac{dn_i}{dt} \qquad .. 15$$

Only the last two transient terms are relevant for localized excited states where $\kappa = \sigma = D = 0$, whereas all terms are appropriate for free carrier excitation. The last term should be summed over all electronic states involved in the transport process. The electric displacement generated

at any point in the crystal at a time t after the light is turned on is

$$\Delta D = \int_0^t J dt \qquad .. 16$$

Since all pyroelectric cyrstals are also electro-optic the electric displacement gives rise to a change of refractive index given by (18)

$$\Delta n_i = \frac{1}{2} n_i^3 r_{ij} \Delta E \qquad .. 17$$

where r_{ij} is the electro-optic coefficient.

Changes of the refractive index due to optically generated electric displacement are referred to as the photorefractive effect by analogy with the term photochromics for optically induced color change.

Optically induced index changes which persisted for long times after the light was turned off were first observed at the focus of intense laser beams in $LiNbO_3$ and $LiTaO_3$ in the absence of applied fields (19). Chen studied the effect in both unbiassed $LiNbO_3$ (4) and in $K(Ta,Nb)O_3$ (20) with an applied electric field. He attributed the index changes to the drift of photoexcited carriers to trapping sites. The resulting inhomogeneous distribution of space charge fields giving rise to the index changes via Eq. 17. Subsequent studies have demonstrated the photorefractive effect in a wide variety of pyroelectric crystals and ceramics, the permanence of the index change and sensitivity to exposure varying widely from one material to another. At the present time it appears that most of the observations can be adequately accounted for by Eqs. 15-17. The magnitude of the persistent index change depends on the photocurrent density J and on the availability of suitable deep traps so that the displaced carriers do not return to their original sites when the light is turned off. J depends firstly on the density of excited photocarriers and secondly on the efficiency of the transport process. Free electrons or holes may be created by linear absorption from the valence to conduction band or transitions from

a defect to the conduction or valence bands. Alternatively at higher intensities free carriers may be created by two photon band-to band transitions via virtual or real intermediate states or by two step absorption at a defect site. Most studies of the photorefractive effect have involved linear absorption by charge transfer from defects. For instance, as we have already seen doping $LiNbO_3$ with Fe^{2+} impurities introduces charge transfer absorption in the blue and green regions of the spectrum where the host crystal is transparent. Consequently the photorefractive sensitivity can be greatly increased (21,22) over nominally pure crystals (which nevertheless have sufficient Fe^{2+} impurities to give significant index changes). Furthermore iron impurities are stable in both di- and trivalent states so that Fe^{3+} impurities which do not absorb in the visible spectrum can act as electron traps. The net result is a spatial variation of the Fe^{2+}/Fe^{3+} ratio. Several other impurities have been shown to sensitize $LiNbO_3$ to optically induced index changes, (22) as well as schemes involving more than one defect **(23)**. Index changes have also been created in undoped $LiNbO_3$ (24) and KTN (25) by two photon transitions from the valence to conduction bands even though the crystal is transparent to the fundamental wavelength. The nature of the traps was not identified.

In iron doped $LiNbO_3$ we have seen that the bulk photovoltaic effect dominates the transport of carriers excited with visible light. Even for applied fields up to 10^4 V/cm photoconductivity plays a small role. The saturation photovoltage of about 10^5 V/cm gives rise to an index change of $\Delta n \sim 10^{-3}$ consistent with early results. (4) Corresponding measurements of the index change and photocurrent in a variety of crystals have verified the photovoltaic origin of the effect. (8) Diffusion currents are smaller than the photovoltaic current for spatial frequencies up to about 10^5 lines/cm, but in materials with a smaller constant κ the effects of diffusion could become significant at practical spatial frequencies. (26)

In KTN on the other hand the photovoltaic effect is zero in the cubic phase and photoconductivity is dominant. Typical measurement of the normalized photocurrent response i/I and absorption coefficient are

shown in Fig. 7. The Curie temperature of this material is 15°C, and measurements were made at 25°C, where the material is highly polarizable.

A useful measure of the photorefractive sensitivity S to compare different materials is the index change per absorbed energy density αW (= $\int \alpha I dt$) i.e.

$$S = \Delta n/\alpha W \qquad .. 18$$

or alternatively this can be written as the electronic displacement $e\ell$ created per absorbed photon. Using Eq. 18 and taking $\Delta E = e\ell\alpha W/\varepsilon\varepsilon_o h\nu$ we find

$$\frac{e\ell}{h\nu} = \left(\frac{\Delta n}{\alpha W}\right)\left(\frac{2\varepsilon\varepsilon_o}{n_i^3 r_{ij}}\right) \qquad .. 19$$

These quantities, evaluated from photorefractive measurements are compared in Table I for unbiased $LiNbO_3$ and KTN with a 6.3 KV/cm bias. The measurement on doped $LiNbO_3$ was made at 0.5145 μm while on the undoped crystals

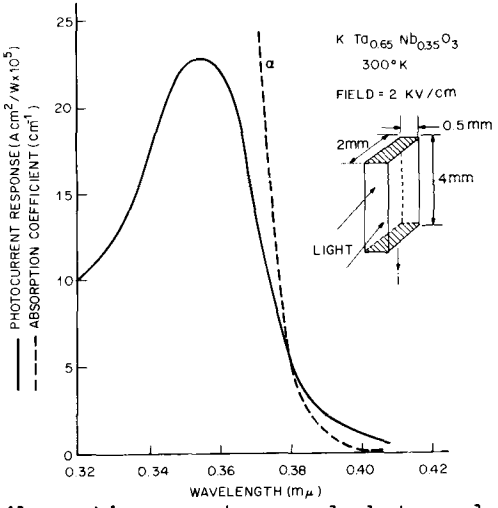

Fig. 7. Absorption spectrum and photoconduction current response i/I of a $K(Ta_{0.65}Nb_{0.35})O_3$ single crystal with an applied field of 6 kV/cm.

Table I. Comparison of the Charge Displacement $e\ell$ Per Excited Carrier and the Photorefractive Sensitivity of $LiNbO_3$ and KTN

Crystal	λ(nm)	$e\ell$ (Debye)	S = cm^3/J
$LiNbO_3$:Fe	515	2.3	1.4×10^{-5}
$LiNbO_3$:Pure	265	6.5	2×10^{-5}
KTN	265	5.6×10^{5}	0.1

measurements were made by two photon absorption of 0.53 μm radiation. It is clear that the photorefractive sensitivity of KTN exceeds that of $LiNbO_3$ by some four orders of magnitude, and it is evident that the difference is due to the much larger distance traveled by the excited carrier in KTN before it is trapped. This result is consistent with the photoconductivity data of Fig. 13. In the wavelength range shorter than 0.38 μm where all the incident energy is absorbed, the photocurrent response of KTN may be written

$$\frac{i}{I} = \frac{d}{h\nu} e\ell \qquad .. 20$$

where d is the width of the illuminated region of crystal. At about 0.35 μm the peak photocurrent response of 23×10^{-6} Acm^2/W gives $e\ell \sim 7\times10^5$ Debye.

In $LiNbO_3$ the value of $e\ell$ is comparable with that expected from local changes of dipole moment $\Delta\mu$ in the absence of space charge fields - namely the difference of dipole moment of unit cells containing an empty or an occupied trapping state as proposed by Johnston (10). However in this case the maximum possible polarization change is $N_D\Delta\mu$ where N_D is the total donor concentration. Saturation index changes of 10^{-3} then require about 10^{20} donors/cc where $\Delta\mu \sim 3$ Debye. However, by photovoltaic transport which gives rise to large space charge fields, each donor can be excited more than once and can contribute a charge displacement of $e\ell$ per

excitation so the required donor density is much smaller.

Index changes based on optically generated space charge fields only persist for the dielectric relaxation time $\tau_r = \varepsilon\varepsilon_0/\sigma$ of the material. The rapid relaxation (27) of Δn in $BaTiO_3$ can be attributed to the high dark conductivity of this material. In pure $LiNbO_3$ the dark resistivity may be greater than 10^{18} ohm cm giving $\tau_r > 40$ days, (28) although this is considerably reduced in doped crystals (see section IV). At temperatures above 100°C the conductivity increases rapidly so the index change disappears in a few seconds. The index change may also be erased by photoconductivity with uniform illumination of crystals. In materials with large photovoltaic effects uniform illumination erases the spatially varying index changes, but instead creates large uniform electric fields unless the crystal is short circuited across the illuminated region. Uniform fields approaching E_{sat} will reduce the photorefractive efficiency for subsequent index changes. This situation does not arise in materials where photoconductive transport is the dominant transport mechanism if erasure is effected in the absence of an applied field. Since the photoconductivity can be varied without affecting κ (See section III) writing and optical erasure of the index change do not necessarily require the same exposure. However it can be shown (29) that the energy required to record the index change cannot be greater than that required to erase it.

While permanent index changes have been emphasized in this section it is appropriate to mention index changes due to the transient terms in Eq. 15. Δn is still given by Eqs. 15, 16 and 17, but in this case there is no macroscopic motion of charge. Consequently any spatial variation of polarization must be accompanied by depolarization fields. Consider the index change created in the form of a diffraction grating by illuminating the crystal with two plane waves interfering at an angle such that the spacing of the grating is small compared with the illuminated area. If the polar axis is normal to the grating planes the depolarization field replicates, but has opposite sense to the excited state polarization, so at all points

$$\frac{dD_3}{dz} = \varepsilon\varepsilon_o \frac{dE_3}{dz} + \frac{dP_3}{dz} = 0$$

An index change due to the electro-optic effect will result from the depolarization fields. However with the perpendicular orientation (Fig. 14b) where the x-axis is normal to the grating and the polar axis lies along the grating lines then div P = 0 in the bulk of the crystal, and depolarization fields due to the crystal surfaces are essentially uniform in the bulk and do not replicate the polarization pattern. Consequently there is no electro-optic index change. Diffractive scattering (30) from such gratings recorded by excitation of localized states in Cr^{3+} doped $LiNbO_3$ show this orientation dependence. The diffraction efficiency of $LiNbO_3$:Cr is consistent with Eqs. 15-17 and the excited state dipole moments determined by the results of section II. The transient index change relaxed with the lifetime of the Cr^{3+} ion excited state. In these experiments the pyroelectric effect could be neglected since the thermal diffusion time was much faster than the electronic relaxation time, so that the thermally induced induced index changes were essentially uniform and did not contribute to the scattering.

VI. Applications

a) Transient Polarization Changes

Application of the pyroelectric effect to the detection of infrared radiation has received a great deal of attention for several years for low frequency thermal detection, and calorimetry as well as for the detection of short optical pulses. The ultimate frequency limitation of the pyroelectric effect is the rate at which the absorbed energy thermalizes in the crystal.

The importance of the electronic polarization change discussed in section II from a practical point of view is that a polarization, which is proportional to the absorbed energy, can be generated at electronic transition rates. As a result, the current density reproduces the

incident pulse shape, and is independent of frequency above the reciprocal electronic relaxation time. i.e.

$$J = \frac{\alpha \Delta \mu}{h\nu} I(t) \qquad .. 21$$

The detection of picosecond optical pulses from a mode locked Nd-glass laser has been demonstrated with Cu^{2+} impurities in $LiTaO_3$. (31) These impurities introduce absorption at 1.06 μm due to the localized $^2E - {}^2T_2$ transition between d-states of the Cu^{2+} ion, the relaxation time of the $^2T_2$ state being about 30 p secs at room temperature. The resulting current pulses were about 10 picoseconds in duration and 250 V amplitude (across 50 ohm) which was consistent with an electronic displacement of about 3 Debye upon excitation.

The absence of power requirements for this kind of detector may prove useful in certain circumstances. For instance pyroelectric waveguides for integrated optical applications could incorporate suitable impurities as an integral part of the waveguide. The feasibility of performing optical switching and logic operations with optical pulse energies of about 20 nJ per gate has been demonstrated (32) in $LiNbO_3$ by directly coupling such a detector to a transparent electro-optic modulator of the same material.

Because of the high frequency response of these devices optical mixing with difference frequencies in the microwave and millimeter wave regions of the spectrum is possible. If two incident beams ω_1 and ω_2 interfere in the absorbing crystal the rapidly varying current density re-radiates at the difference frequency $\omega_3 = \omega_1 - \omega_2$. If the absorption depth of the material is smaller than the coherence length of the interaction of the three beams (i.e. $\alpha >> \omega_3 (n_1 - n_3)/\pi c$ where n_1, n_3 are the refractive indices at ω_1 and ω_3), then phase matching can be avoided.

An experiment of this kind was performed with heavily reduced $LiNbO_3$ crystals which were highly absorbing in the visible region of the spectrum ($\alpha \sim 200$ cm^{-1}) irradiated with two tunable dye lasers. (33)

By tuning the dye lasers the difference frequency ω_3 could be tuned continuously from 2 cm^{-1} to 50 cm^{-1}. The peak for infrared output intensity was about 2 mW for 150 kW/beam input - considerably greater than that obtained by using the electro-optic effect in transparent crystals. An advantage of using the excited state dipole for far infrared generation is that the complications of phase matching by angle or temperature tuning the birefringence can be avoided by increasing α without loss of conversion efficiency since $J \propto \alpha$ (see Eqn. 21).

It should be noted that optical rectification experiments lend themselves quite well to the measurement of $\Delta\mu$ of very short lived states. Comparison of the total microwave output of the absorbing crystal with a known reference crystal when both are excited with short optical pulses (see Fig. 8) gives a direct measurement of $\Delta\mu$ associated with the absorbing center providing that the electronic relaxation time is long compared with the input pulse duration and the low frequency cut off of the microwave detection system.

b) Photovoltaic Effects

At the present time the power conversion efficiency of the photovoltaic effects discussed in sections III and IV are too small for these materials to be considered for energy conversion applications - particularly in view of

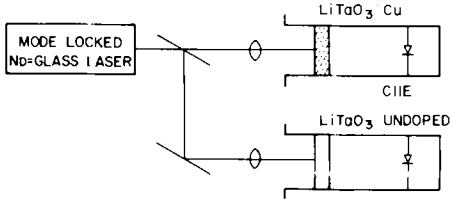

Fig. 8. Experimental arrangement for the comparison of excited state dipole moments in systems with short excited state lifetimes.

the high photovoltaic efficiencies of semiconducting junctions. Furthermore, for detector applications the current responsivity is too small to be practical. On the other hand the extremely high voltages which can easily be generated with small light intensities may be useful for applications with low electrical power requirements. For instance the construction of a megavolt generator with no electrical power requirements appears to be quite feasible with relatively small ($\sim$ 10 cm) crystals of $LiNbO_3$.

c) Photorefractive Effects

Optically induced index changes in electro-optic materials have attracted considerable interest for optical memory applications. The useful features of this effect for information storage is its reversibility, high resolution and linearity with exposure. As we have seen in section V, saturation of the photocurrents in $LiNbO_3$ do not occur until $\Delta n \sim 10^{-3}$. The bit density is limited only by the diffraction of light. Information can be recorded in a bit-by-bit fashion with a focused laser beam or else an entire image can be recorded at once. (34) Readout of the induced retardation may be accomplished with light of a different wavelength than that used for writing.

Holographic recording on the other hand has the advantage that fewer optical components (no compensator or analyzer) are required and that much higher storage densities can be achieved, particularly if several holograms are superimposed in the same volume of material, and since each bit of information is spread over the entire illuminated region of the crystal, the effect of dust spots and crystal defects is minimized.

The arrangement for recording an elementary phase hologram using the photorefractive process is shown in Fig. 9. The sinusoidal interference pattern of the two plane waves creates a sinusoidal index variation in the crystal. Free charge generated in the regions of high intensity is displaced toward regions of lower intensity where it is trapped. To read the information one of the beams is diffracted from the hologram, the diffraction efficiency being given by (35)

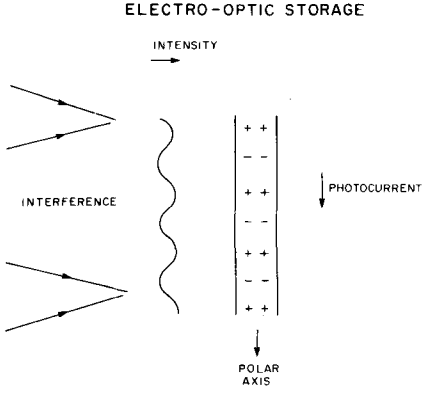

Fig. 9. Arrangement for recording an elementary hologram using the photorefractive effect.

$$\eta = e^{-\alpha d} \sin^2 \frac{\Delta n l \pi}{\lambda \cos\theta} \qquad .. 22$$

where θ is the angle between the writing beams. To reconstruct a hologram consisting of several spatial frequencies, the same wavelength of light must be used for reading as for writing in order to satisfy the Bragg conditions. It is clear from Eq. 22 that diffraction efficiencies approaching 100% are possible in weakly absorbing crystals. For maximum index change per exposure however, Eqs. 15-17 show that a high absorption is desirable, the optimum crystal transmission being 33%. Comparison of Eqs. 22 and 18 shows that a material with a large photorefractive sensitivity is desirable for these applications. The maximum possible sensitivity is obtained when the **drift** length of the photoexcited electron is comparable to the interference fringe spacing. From Table I we see that KTN approaches this limit with 6 KV/cm. A diffraction efficiency of about 5% was obtained (25) for an exposure of 100 $\mu J/cm^2$. At the present time it appears that photoconductivity is a more

efficient mechanism for optical storage than the photovoltaic effect. In ferroelectric $Sr_{1-x}B_xNb_2O_6$ (SBN) photoconductivity also gives a high photorefractive sensitivity. (36) Nevertheless for optical storage other requirements of the storage medium are long storage time and high crystal quality. With both KTN and SBN, crystals of high optical quality are difficult to grow and the dark conductivity at room temperature is moderately high so that storage times of only a few hours are possible. Cooling crystals should result in longer storage times. $LiNbO_3$ on the other hand has a much lower photorefractive sensitivity, even when sensitized with dopants, yet crystals of high optical quality are readily obtained and the dark conductivity is considerably lower than KTN.

A further practical problem is that readout with the same wavelength of light used for writing tends to erase the stored information. The relative sensitivity to writing and erasure may be varied in $LiNbO_3$ by varying the ratio σ/κ as discussed in section V, but a method for avoiding unwanted erasure entirely is by two photon absorption for recording and erasure: Namely, by writing the hologram at frequency ω_1 to which the material is insensitive, in the presence of a second frequency ω_2 which carries no information. The combined energy $\omega_1 + \omega_2$ is sufficient to excite photocurrents. Reading is then performed at ω_1 as required by the Bragg conditions. Alternatively, the electronic charge pattern may be 'fixed' by ionic conductivity (28) or polarization reversal (37) in regions of high space charge field. Holograms fixed in this way are very stable yet thermal or electrical erasure is still possible.

In a few applications - such as real time holographic interferometry or signal processing - long storage times may be undesirable. In such cases the transient photorefractive effect due to localized excitation may be of use.

In each of these applications the primary requirement of the materials and the defects is that a large electric displacement be generated by the incident light. The larger the displacement, in general, the more efficient

the device. Of course in photoconductive materials large displacement may be obtained in materials polarized in an external field. The main purpose of this paper has been to discuss how even in the absence of macroscopic fields the absorption of light in pyroelectric crystals can give rise to both transient and steady state photocurrents which are essentially driven by the microscopic fields at the defect sites, and which open up some new possibilities for application as well as for fundamental study. The large range of materials at our disposal include pyroelectric crystals, ceramics and polymers and piezoelectrics under stress.

Acknowledgments

We would like to acknolwedge helpful discussions with D. A. Kleinman concerning the bulk photovoltaic effect with pyroelectrics.

References

1. A. G. Chynoweth, Phys. Rev. 102, 705 (1956).

2. A. Lempicki, Phys. Rev. 113, 1204 (1959).

3. P. S. Brody, Solid State Comm. 12, 673 (1973).

4. F. S. Chen, J. Appl. Phys. 40, 3389 (1969).

5. I. I. Goldman, V. D. Krivechenkov, V. I. Kogan and V. S. Galiskii, "Problems in Quantum Mechanics" ed. D. ter Haar, Academic Press, N. Y. (1960).

6. A. M. Glass and D. H. Auston, Optics Comm. 5, 45 (1972).

7. A. M. Glass and D. H. Auston, unpublished data.

8. A. M. Glass, D. von der Linde and T. J. Negran, Appl. Phys. Lett. 25, 233 (1974).

9. M. G. Clark, F. J. Di Salvo, A. M. Glass and G. E. Peterson, J. Chem. Phys. 59, 6209 (1973).

10. W. D. Johnston, Jr., J. Appl. Phys. 41, 3279 (1970).

11. S. G. Ellis, F. Herman, E. E. Loebner, W. J. Merz, C. W. Struck and J. G. White, Phys. Rev. 109, 1860 (1958).

12. W. J. Merz, Helv, Phys. Acta 31, 625 (1958).

13. G. F. Neumark, Phys. Rev. 125, 838 (1962).

14. G. Cheroff and S. P. Keller, Phys. Rev. 111, 98 (1958).

15. L. Pensak, Phys. Rev. 109, 601 (1958); B. Goldstein, ibid, 601 (1958).

16. A. R. Auston, Bull. Amer. Phys. Soc. II6, 110 (1961).

17. A. M. Glass and T. J. Negran, unpublished data.

18. F. Pockels, "Lehrbuch der Kristalloptik" part IV, chapter 3, p. 492, Teubner, Leibzig 1906.

19. A. Ashkin, G. D. Boyd, J. M. Dziedzic, R. G. Smith, A. A. Ballman, H. J. Levinstein and K. Nassau, Appl. Phys. Lett. 9, 72 (1966).

20. F. S. Chen, J. Appl. Phys. 38, 3148 (1967).

21. G. E. Peterson, A. M. Glass and T. J. Negran, Appl. Phys. Lett. 19, 130 (1971).

22. W. Phillips, J. J. Amodei and D. L. Staebler, RCA Rev. 33, 94 (1972).

23. D. L. Staebler and W. Phillips, Appl. Phys. Lett. 24, 268 (1974).

24. D.von der Linde, A. M. Glass and K. F. Rodgers, Appl. Phys. Lett. 25, 155 (1974).

25. D. von der Linde, A. M. Glass and K. F. Rodgers, Appl. Phys. Lett. 26, 22 (1975).

26. J. J. Amodei, RCA Rev. 32, 185 (1971).

27. R. L. Townsend and J. T. LaMacchia, J. Appl. Phys. 41, 5188 (1970).

28. D. L. Staebler and J. J. Amodei, Ferroelectrics 3, 107 (1972).

29. D. L. Staebler and W. Phillips, Appl. Opt. 13, 793 (1974).

30. A. M. Glass and D. von der Linde, to be published.

31. D. H. Auston and A. M. Glass, Appl. Phys. Letters 20, 298 (1972).

32. A. M. Glass and T. J. Negran, Appl. Phys. Letters 24, 81 (1974).

33. D. H. Auston, A. M. Glass and P. LeFur, Appl. Phys. Lett. 23, 47 (1973).

34. J. Feinleib and D. S. Oliver, Applied Optics 11, 2752 (1972).

35. H. Kogelnik, Bell System Tech. J. 48, 2909 (1969).

36. J. B. Thaxter and M. Kestigian, Appl. Opt. 13, 913 (1974).

37. F. Micheron, C. Mayeux and J. C. Trotier, Appl. Opt, 13, 784 (1974).

38. J. G. Bergman, Jr., J. H. McFee and G. R. Crane, Appl. Phys. Lett. 18, 203 (1971).